MRS Advances

Characterization of thin CdTe solar cells with a CdSeTe front layer

Alexandra M. Bothwell, Jennifer A. Drayton, Pascal M. Jundt, and James R. Sites

Colorado State University, Fort Collins, CO 80523, U.S.A.

ABSTRACT

Thin CdTe photovoltaic device efficiencies show significant improvement with the incorporation of a CdSeTe alloy layer deposited between a MgZnO emitter and CdTe absorber. CdTe and CdSeTe/CdTe devices fabricated by close-space sublimation with a total absorber thickness of 1.5 µm are studied using microscopy measurements and show minimal diffusion of Se into the CdTe. Current loss analysis shows that the CdSeTe layer is the primary absorber in the CdSeTe/CdTe structure, and fill factor loss analysis shows that ideality-factor reduction is the dominant mechanism of fill factor loss. Improvement in the CdSeTe/CdTe absorber quality compared to CdTe is also reflected in spectral and time-resolved photoluminescence measurements. Current density vs. voltage measurements show an increase in current density of up to 2 mA/cm² with the addition of CdSeTe due to a band gap shift from 1.5 to 1.42 eV for CdTe and CdSeTe/CdTe absorbers respectively. Voltage deficit is lower with the incorporation of the CdSeTe layer, corroborated by improved electroluminescence intensity. The addition of CdSeTe into CdTe device structures has increased device efficiencies from 14.7% to 15.6% for absorbers with a total thickness less than two microns.

INTRODUCTION

Cadmium telluride (CdTe) is an advantageous absorber material for photovoltaic applications because its favourable absorption coefficient allows for an ultra-thin absorber layer, which reduces deposition time and fabrication costs [1]. CdTe photovoltaic devices have demonstrated immense improvement in the past decade with efficiencies reaching 18.6% and 22.1% for modules and research-based small area devices respectively [2, 3]. Rapid progress is due in part to developments in device architecture, such as the incorporation of a cadmium selenium telluride ($CdSe_{1-x}Te_x$) alloy into the absorber layer.

A CdSeTe/CdTe bilayer absorber improves photovoltaic efficiency compared to a single CdTe absorber by increasing the short-circuit current density (J_{SC}) of the device.

Due to a 100-meV narrower bandgap than CdTe, the CdSeTe layer increases photon absorption above the conduction band, thus improving current collection [4]. Se also passivates bulk defects in the absorber, leading to increased device performance [5]. Previous work has shown successful incorporation of CdSeTe and good performance using a CdSeTe/CdTe bilayer, however, only for absorbers greater than 4.0 µm with CdSeTe purposefully diffused into the CdTe layer [4]. This study demonstrates that a 1.5 µm CdSeTe/CdTe absorber with no intentional diffusion offers the same performance benefits as its thicker counterpart. We also look in greater detail at why the bilayer absorber is much better than a single CdTe absorber using current and fill factor loss analysis.

EXPERIMENT

Device fabrication

Two device structures were explored in this work: one with a CdTe absorber and the other with a CdSeTe/CdTe bilayer absorber. Devices were fabricated in a superstrate configuration on commercially-made Tec10, a 3.2 mm soda-lime glass coated with a SnO_2:F transparent conducting oxide (TCO) layer. A 100-nm $Mg_xZn_{1-x}O$ (MZO) emitter layer, deposited by RF magnetron sputtering, was used as the n-type window layer for its favorable optical properties and band alignment with the absorber layer [6]. The p-type CdSeTe alloy and CdTe layers were deposited on the MZO by close-space sublimation (CSS) in a fully automated, single-vacuum system [7]. The single CdTe absorber was 1.5 µm and the bilayer was composed of 0.5-µm CdSeTe with 20% CdSe molar fraction in the source material followed by 1.0-µm CdTe, where the thickness of the absorber layers was controlled by sublimation time.

An optimized cadmium-chloride ($CdCl_2$) passivation treatment of the absorber layers, known to promote grain growth, passivate grain boundaries, and improve device performance in CdTe films [8, 9] was carried out in the same co-sublimation system. The $CdCl_2$ treatment has also been used to promote CdSeTe/CdTe interdiffusion in thicker absorbers [4, 5]. With the thinner absorbers, however, the treatment was less aggressive, and there was less interdiffusion. The $CdCl_2$ deposition time was 150 seconds followed by a 300-second anneal; the source temperatures were 437°C and 400°C respectively. After cooling, plates were removed from the vacuum system and rinsed with deionized water to remove residual $CdCl_2$ from the film surface. Cu doping of the films was carried out in a separate CSS system, followed by a 40-nm evaporated Te buffer layer and a ~140-µm colloidal Ni paint back contact [10]. Twenty-five small-area devices (~0.65 cm^2) were delineated for each superstrate. Reproducibility is high; efficiency variation is less than 0.3% absolute between successive depositions. The completed device structures for the CdTe and CdSeTe/CdTe absorbers are shown in Figures 1 (a) and (b), respectively.

Characterization

Material analysis was performed on films terminated at the Te layer. Cross-sectional scanning transmission electron microscopy (STEM) was used to image the CdSeTe/CdTe film prepared by focused ion beam (FIB) milling, accompanied by energy-dispersive X-ray spectroscopy (EDS) analysis. Time-of-flight secondary ion mass spectrometry (SIMS) was measured on the bilayer absorber structure with a 30 keV primary ion beam and a thermal ionization cesium sputtering source. Room-temperature photoluminescence emission spectroscopy (PL) was measured from the glass-side of completed devices with a 520-nm excitation laser and 570-nm long pass filter to minimize any signature from the excitation source. Single-photon time-resolved photoluminescence

(TRPL) was also measured from the glass-side of completed devices with an excitation wavelength of 640 nm, 1-mW average power, 1.1-MHz repetition rate, and a beam diameter of 0.3 mm. TRPL emission was measured with an 819 and 870 nm-centered bandpass filter for the CdTe and CdSeTe/CdTe absorbers respectively.

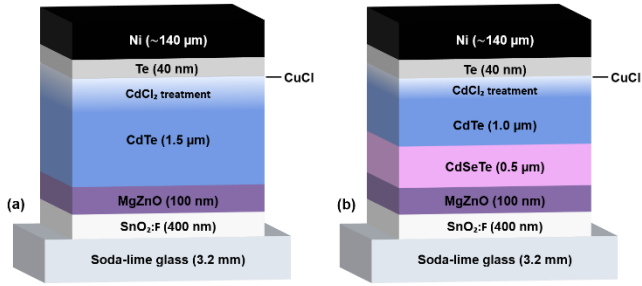

Figure 1. Device structure of CdTe (a) and CdSeTe/CdTe (b) absorbers where light is incident on the glass-side.

Completed devices were characterized under standard test conditions including external quantum efficiency (QE) and current density-voltage (J-V) measured using a Solar Light Co. XPS 400 xenon lamp AM 1.5 solar simulator. Optical reflection and transmission were measured using a Perkin Elmer Lambda 2 spectrophotometer. Electroluminescence (EL) imaging was done on best-performing devices in a light-tight enclosure with a Finger Lakes MicroLine ML8300 Si CCD camera operated at -25°C to minimize thermal noise [11]. EL images were normalized to exposure time and injection current density (100 seconds and 20 mA/cm^2 respectively), scaled logarithmically, and color-mapped.

RESULTS

Material characterization

Structures fabricated with CdTe on MZO maintain a continuous MZO layer and have fairly large grains that extend through the absorber [12]. To investigate how the introduction of CdSeTe affects film structure, cross-sectional STEM of CdSeTe/CdTe on MZO was imaged and is shown in Figure 2. Deposition of CdSeTe onto MZO does not appear to alter the emitter layer: the MZO is continuous across the film cross section, and the MZO/CdSeTe interface is like that seen for MZO/CdTe. The bilayer absorber grains are fairly large, with many extending throughout the full absorber, similar to that of CdTe, and the grain structure shows no indication of grain-formation differences between the CdSeTe and CdTe layers.

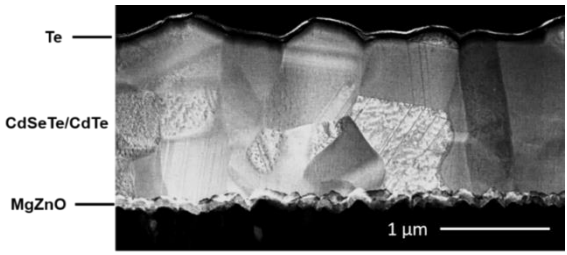

Figure 2. Cross sectional STEM of CdSeTe/CdTe structure shows fairly large absorber grains and continuous MZO.

To confirm the incorporation of the CdSeTe and quantify elemental diffusion, SIMS measurements were performed on the $CdCl_2$-treated CdSeTe/CdTe bilayer structure and are shown in Figure 3. Given elements are the most abundant isotope except for Se, which uses $^{78}Se+$ to eliminate a mass overlap with ZnO+. The Se profile shows a decrease in intensity midway through the absorber with a corresponding drop in Te:Cd ratio, which verifies that the CdSeTe alloy is incorporated at the front of the absorber with only a small amount of diffusion into the CdTe. The CdSeTe to CdTe transition is not abrupt but is sufficiently narrow (<50 nm) that the term bilayer is appropriate. EDS line scans were also measured on this structure and confirmed CdSeTe incorporation and minimal interdiffusion.

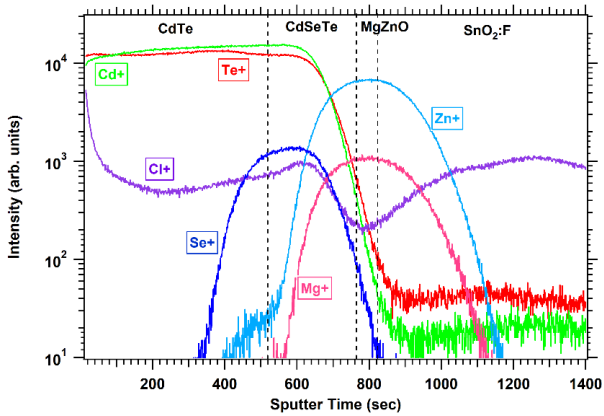

Figure 3. SIMS profiles of the CdSeTe/CdTe structure measured with a Cs+ sputtering source show little CdSeTe/CdTe interdiffusion or Mg and Zn diffusion.

The width of the Mg and Zn peaks cannot be used to accurately quantify the thickness of the MZO layer because the sputter rate of oxides is slower than that of the absorber, therefore the symmetry of the Mg and Zn profiles is used to identify elemental diffusion. In this case the Mg and Zn peaks are fairly symmetric and show little sign of diffusion into the absorber layer.

The bandgap of the CdTe and CdSeTe/CdTe structures is determined by dQE/dE and PL measured as a function of energy as shown in Figure 4 (a). The data show a clear shift in bandgap from 1.5 eV to 1.42 eV with the incorporation of the CdSeTe alloy into the absorber. The six-fold increase in PL intensity for CdSeTe/CdTe compared to CdTe suggests the CdSeTe has more favorable material properties since PL intensity is associated with external radiative efficiency.

TRPL decays of the CdTe and CdSeTe/CdTe structures given in Figure 4 (b) show clear improvement in tail lifetime with the incorporation of CdSeTe into the absorber. The tails of the decay data were fit with an x-offset exponential function and the extracted tail lifetimes were 1.6 ± 0.02 ns and 12.6 ± 0.1 ns for the CdTe and CdSeTe/CdTe

structures respectively. The minimum lifetime that can be measured due to inherent equipment delay is 0.3 ns.

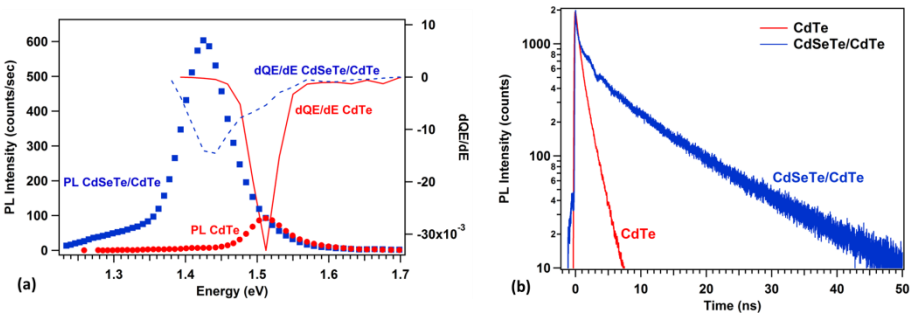

Figure 4. Spectral PL and the derivative of quantum efficiency as a function of energy are used to determine absorber bandgap (a). Time-resolved photoluminescence shows greatly improved tail lifetime for the CdSeTe/CdTe structure (b).

Device characterization

The thin CdSeTe/CdTe bilayer absorbers show improved device performance compared to devices with a single CdTe absorber as demonstrated by the J-V curves of the best-performing devices shown in Figure 5. The corresponding J-V parameters are given in Table I which also provides the mean and standard deviation of the five best-performing devices for each plate.

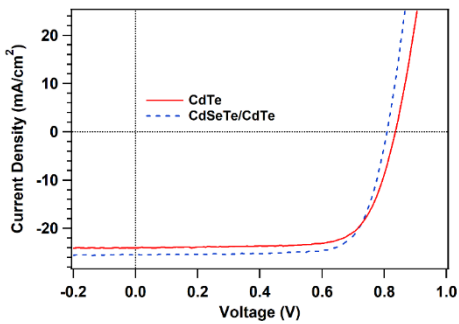

Figure 5. Light J-V curves of the best-performing CdTe and CdSeTe/CdTe devices.

Due to the narrowed bandgap and passivating effects of the CdSeTe/CdTe absorber, J_{SC} increases with the incorporation of CdSeTe. The fill factor also improves for the bilayer absorber. These two parameters drive the 6% relative increase in efficiency for the CdSeTe/CdTe device. The open circuit voltage (V_{OC}) decreases with the incorporation of CdSeTe because of the narrower absorber bandgap. However, due to the difference in bandgap, the maximum attainable V_{OC} is different for the single versus bilayer absorber. The authors believe that a more useful metric to consider is voltage deficit: the difference between the maximum and measured V_{OC}. As is given in Table I, the CdSeTe/CdTe structure has a lower voltage deficit than the CdTe structure. Since EL intensity is inversely proportional to voltage deficit [11], the improvement in voltage deficit can also be highlighted by EL measurements. EL of the CdTe device given in Figure 6 (a) shows less EL intensity than the CdSeTe/CdTe device in Figure 6 (b), which again indicates that the bilayer absorber better minimizes the voltage deficit.

Table I. J-V parameters of best-performing CdTe and CdSeTe/CdTe devices and mean and standard deviation of the five best-performing devices.

Absorber	J_{SC} (mA/cm^2)	V_{OC} (V)	$V_{deficit}$ (V)	FF (%)	η (%)
Best CdTe	24.0	0.835	0.365	73.4	14.7
Best CdSeTe/CdTe	25.5	0.808	0.342	75.5	15.6
CdTe Mean ± St. Dev.	24.2 ± 0.1	0.835 ± 0.001	0.365 ± 0.001	72.2 ± 0.7	14.6 ± 0.1
CdSeTe/CdTe Mean ± St. Dev.	25.5 ± 0.1	0.810 ± 0.001	0.340 ± 0.001	74.0 ± 1.1	15.3 ± 0.2

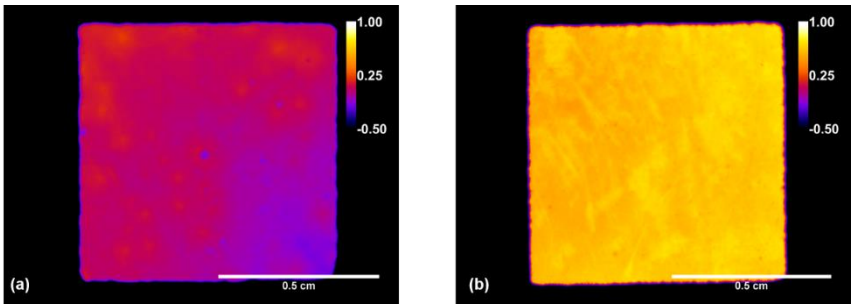

Figure 6. EL images of best-performing CdTe (a) and CdSeTe/CdTe (b) devices shows improved uniformity and EL intensity of the bilayer absorber. Color-mapping scale is the same in both images.

Loss analysis

The difference in fill factor between the single and bilayer absorber devices can be quantified using loss analysis techniques described in [13]. The relationship between the measured fill factor and the maximum theoretical fill factor is given by equation 1.

$$FF_{meas}=\alpha_1\alpha_2\alpha_3\alpha_4\alpha_5 FF_0 \quad (1)$$

where α_i is the fractional loss from different mechanisms and FF_0 is the ideal fill factor. FF_0 is calculated based on the absorber bandgap and is 89.8% and 89.4% for CdTe and CdSeTe/CdTe respectively. The fractional losses correspond to reduced V_{OC}, non-ideal diode quality factor (A), series resistance (R_S), shunt conductance (G), and other losses. As Hegedus and Shafarman describe [14], manipulation of the J-V data can be done such that linear fits allow for extraction of A, R_S, and G, and these parameters can be converted to fill factor losses. This technique was used for the best CdTe and CdSeTe/CdTe devices given in Table I, and the fill factor loss analysis results are given in Figure 7. The ideality-factor reduction constitutes the largest component of fill factor losses, with series resistance and V_{OC} reduction making up a smaller portion for both devices.

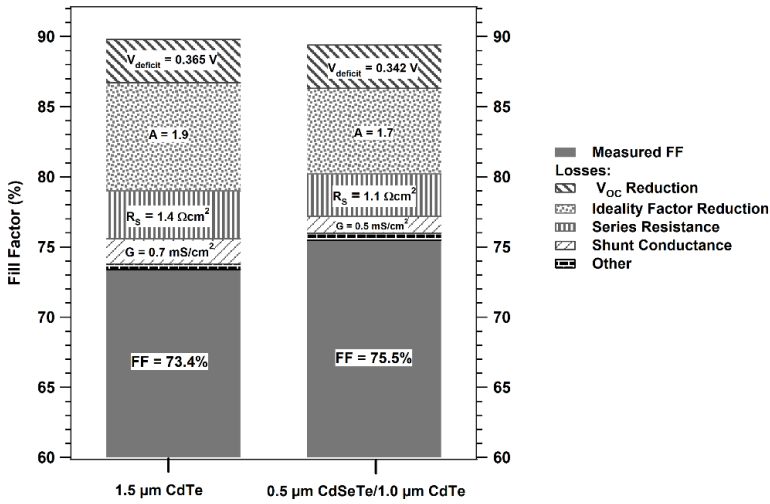

Figure 7. Fill factor losses analyzed for separate mechanisms for CdTe and CdSeTe/CdTe devices.

Since there is a large boost in J_{SC} with the addition of CdSeTe to the absorber, it is also useful to quantify the current losses for a CdTe and a CdSeTe/CdTe device. Measured J_{SC} of the device is determined by the integral over wavelength of the product of the measured QE with the AM 1.5G spectrum and the maximum theoretical J_{SC} is determined based on 100% QE and the absorber bandgap. The difference between the maximum theoretical and measured J_{SC} is separated into different current loss mechanisms using reflection, transmission, and absorption measurements. The losses are categorized as front-layer absorption (photon absorption in the glass, TCO, and MZO layers), front-surface reflection, incomplete absorption, and recombination. Each is integrated with the AM 1.5G spectrum to determine corresponding current density loss, described in more detail in [14, 15]. In the case of the bilayer absorber, transmission of a 0.5 µm CdSeTe film is used to separate current collected in the CdSeTe and CdTe layers. The current loss analysis results for a thin CdTe and CdSeTe/CdTe absorber are shown in Figure 8 (a) and (b) respectively, and the current density values of each loss are given in Table II. As only one-third of the absorber, CdSeTe is the dominant current collector, accounting for 88% of the current collection.

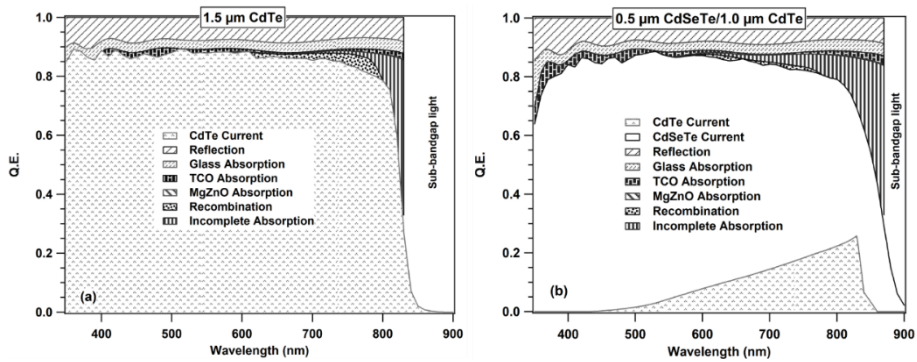

Figure 8. Current density loss analysis for CdTe (a) and CdSeTe/CdTe (b) devices.

Table II. Mechanisms of current density loss in CdTe and CdSeTe/CdTe devices.

Mechanism	CdTe J (mA/cm^2)	CdSeTe/CdTe J (mA/cm^2)
CdTe Current Density	24.6	3.0
CdSeTe Current Density	--	22.9
Reflection Loss	2.3	2.7
Glass Absorption	1.0	1.1
TCO Absorption	0.3	0.5
MZO Absorption	< 0.1	< 0.1
Recombination Loss	0.1	0.1
Incomplete Absorption	0.6	1.3
Max Current Density	**28.8**	**31.5**

DISCUSSION

A CdSeTe/CdTe bilayer absorber shows, with thin absorbers as well as thicker ones previously reported [4], improvements to photovoltaic device performance compared to a single CdTe absorber, due in part to the material properties of CdSeTe. The six-fold increase in peak PL intensity for the CdSeTe/CdTe compared to CdTe absorber is attributed to the CdSeTe layer since the ~0.2 µm absorption depth of the excitation laser probes the CdSeTe. This suggests superior radiative efficiency properties of the CdSeTe material. Changes in TRPL tail lifetime, τ_2, correspond to changes in bulk properties for thin-film CdTe devices [16]. The improvement in τ_2 lifetime for the CdSeTe/CdTe bilayer device shown in Figure 4 (b) suggests that bulk recombination is reduced with the incorporation of CdSeTe.

Although V_{OC} is slightly lower for the CdSeTe/CdTe device, the voltage deficit is lower than that of CdTe as demonstrated in J-V measurements as well as EL intensity. This may be explained in two ways. First, because bulk recombination is a limitation of V_{OC} [17] and TRPL suggests reduced bulk recombination for CdSeTe/CdTe, and Se passivates critical bulk defects [5], a lower voltage deficit may be due to improved bulk material properties of the CdSeTe/CdTe structure. Second, band alignment between the 1.4 eV CdSeTe and 1.5 eV CdTe creates a conduction-band offset at the CdSeTe/CdTe interface, but the same built-in potential is maintained as for CdTe alone [18, 19].

J_{SC} and fill factor increase the efficiency of the CdSeTe/CdTe device, therefore, more in-depth analysis was done on current and fill factor losses. Ideality-factor reduction, resulting from recombination, is the dominant fill factor loss mechanism in both structures. As indicated by photoluminescence measurements, there is less bulk recombination in the bilayer absorber structure, leading to a somewhat lower ideality factor for that device. However, because the CdTe/Te interface has a fairly high surface recombination velocity [20], ideality-factor reduction is still the dominant fill factor loss mechanism independent of absorber. V_{OC} reduction and series resistance are somewhat comparable fill factor loss mechanisms although both are slightly better for the bilayer structure, and losses due to shunt conductance have a minor contribution. To improve fill factor in these devices, the voltage deficit must be reduced further, and bulk and interfacial recombination must be minimized. Current loss analysis reveals that the CdSeTe layer is the dominant absorber, accounting for 88% of current collection in the given bilayer structure and 96% of current collection has been observed with a ~1.0 µm CdSeTe layer. Because the window layers are nominally identical for both absorber structures, the window layer absorption and reflection losses are comparable. Reflection losses can be reduced with the addition of an anti-reflection coating on the front-surface of the glass. Although the CdTe and CdSeTe/CdTe absorbers are the same total thickness, incomplete absorption is a larger source of current loss in the CdSeTe/CdTe device because its narrower bandgap effectively increases the absorption potential of the absorber.

CONCLUSION

1.5 µm CdTe and 0.5 µm CdSeTe/1.0 µm CdTe absorbers were fabricated by CSS to increase device performance of thin CdTe PV structures and quantify the differences between the single and bilayer absorbers. Increased PL intensity and longer TRPL tail lifetimes for the CdSeTe/CdTe structure suggests enhanced radiative efficiency and better bulk properties respectively, indicative of improved absorber material. CdSeTe material properties may be a cause for the lowered voltage deficit in the CdSeTe/CdTe device as demonstrated in both J-V and EL measurements. J-V measurements also show the measured J_{SC} of the CdSeTe/CdTe device is 1.5 mA/cm^2 higher than that of the CdTe device, due to the 100-meV narrower bandgap of CdSeTe compared to CdTe as well as passivating effects of Se. Analysis of current losses for the CdTe and CdSeTe/CdTe devices show that CdSeTe is the dominant absorber. Fill factor loss analysis on the same devices show that ideality-factor reduction dominates fill factor losses for both absorber structures. Increases in J_{SC} and fill factor generate a 15.6%-efficient CdSeTe/CdTe device, among the highest-performing CdTe-based device thinner than 2.0 µm. Thin devices require less material and time to fabricate, and high efficiencies of such thin devices are promising developments to make thin-film CdTe PV more cost competitive.

ACKNOWLEDGEMENTS

The authors would like to thank Professor W.S. Sampath for use of his deposition systems, Kevan Cameron for system support, Dr. Roy Geiss for TEM assistance, and Michael Walker at Colorado School of Mines for SIMS measurements.

This material is based upon work supported by the U.S. Department of Energy's Office of Energy Efficiency and Renewable Energy (EERE) under Solar Energy Technologies Office (SETO) Agreement Number DE-EE0007543. This material makes use of the TOF-SIMS system at the Colorado School of Mines, which was supported by the National Science Foundation under Grant No.1726898.

REFERENCES

[1] B. McCandless and J. Sites, in *Handbook of Photovoltaic Science and Engineering,* edited by A. Luque and S. Hegedus, (John Wiley & Sons Ltd., West Sussex, England, 2003), p. 617-618.
[2] M. A. Green, K. Emery, Y. Hishikawa, W. Warta, and E. D. Dunlop, Prog. Photovolt. **23** (1), 1–9 (2015).
[3] Exclusive: First Solar's CTO discusses record 18.6% efficient thin-film module (2015). Available at: http://www.greentechmedia.com/articles/read/Exclusive-First-Solars-CTO-Discusses-Record-18.6-Efficient-Thin-Film-Mod
[4] A. Munshi et al., IEEE Journal of Photovoltaics **8** (1), 310-314 (2018).
[5] T. Fiducia et al., Nature **4** (6), 504-511 (2019).
[6] J. Kephart, PhD. Thesis, Colorado State University, 2015.
[7] D.E. Swanson et al., Journal of Vacuum Science & Technology A, **34**, (2), 021202, (2016).
[8] A. Abbas et al., Proc. IEEE 40th Photovolt. Spec. Conf., 0701-0706, (2014).
[9] A. Munshi et al., Proc. IEEE 40th Photovolt. Spec. Conf., 1643-1648, (2014).
[10] A. Moore, T. Song, and J. Sites, MRS Advances **2** (53), 3195-3201 (2017).
[11] J. Raguse, PhD. Thesis, Colorado State University, 2015.
[12] A. Munshi et al., Proc. IEEE 42nd Photovolt. Spec. Conf., 0465-0469, (2016).
[13] M. Green, *Solar Cells*, (The University of New South Wales, Kensington, NSW) p. 96-98.
[14] S. Hegedus, and W. Shafarman, Prog. Photovolt.: Research and Appl. 12, 155-176 (2004).
[15] A. Wojtowicz, Master's Thesis, Colorado State University, 2017.
[16] A. Kanevce, et al., Prog. Photovolt.: Research and Appl. 22, 1138-1146 (2014).
[17] D. Kuciauskas et al., IEEE Jour. of Phot., **6**, (1), 313-318 (2016).
[18] J. Sites and P. Jundt, 15th Photovolt. Science, Appl., and Tech Conference, UK, (2019).
[19] T. Song, A. Kanevce, and J. Sites, J. Apppl. Phys. **119**, 233104 (2016).
[20] A. Huss, J. Drayton, and J. Sites, Proc. IEEE 45th Photovolt. Spec. Conf., 3703-3708, (2018).